

High Methane Storage Working Capacity in Metal–Organic Frameworks with Acrylate Links

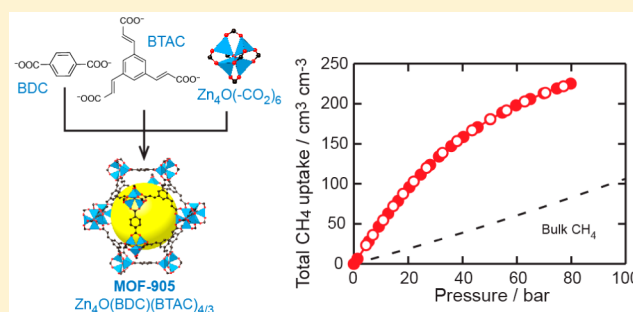
Juncong Jiang,^{†,‡} Hiroyasu Furukawa,^{†,‡} Yue-Biao Zhang,[†] and Omar M. Yaghi^{*,†,§}

[†]Department of Chemistry, University of California—Berkeley; Materials Sciences Division, Lawrence Berkeley National Laboratory; Kavli Energy NanoSciences Institute at Berkeley, Berkeley, California 94720, United States

[§]King Abdulaziz City for Science and Technology, Riyadh 11442, Saudi Arabia

S Supporting Information

ABSTRACT: High methane storage capacity in porous materials is important for the design and manufacture of vehicles powered by natural gas. Here, we report the synthesis, crystal structures and methane adsorption properties of five new zinc metal–organic frameworks (MOFs), MOF-905, MOF-905-Me₂, MOF-905-Naph, MOF-905-NO₂, and MOF-950. All these MOFs consist of the Zn₄O(-CO₂)₆ secondary building units (SBUs) and benzene-1,3,5-tri-β-acrylate, BTAC. The permanent porosity of all five materials was confirmed, and their methane adsorption measured up to 80 bar to reveal that MOF-905 is among the best performing methane storage materials with a volumetric working capacity (desorption at 5 bar) of 203 cm³ cm⁻³ at 80 bar and 298 K, a value rivaling that of HKUST-1 (200 cm³ cm⁻³), the benchmark compound for methane storage in MOFs. This study expands the scope of MOF materials with ultrahigh working capacity to include linkers having the common acrylate connectivity.



INTRODUCTION

Methane, the lightest of hydrocarbons, draws a lot of attention because it has a very high research octane number (RON = 107), yet low CO₂ emissions. It is predicted that the demand of energy from natural gas will exceed 200 exajoules per year in 2040, as the second largest energy source.¹ Although natural gas represents over 60% of the fossil fuels on earth, it remains the least utilized compared to oil and coal. Currently, natural gas is employed mainly as a fuel for electric power plants (31%), industry (28%), and in homes (19%).²

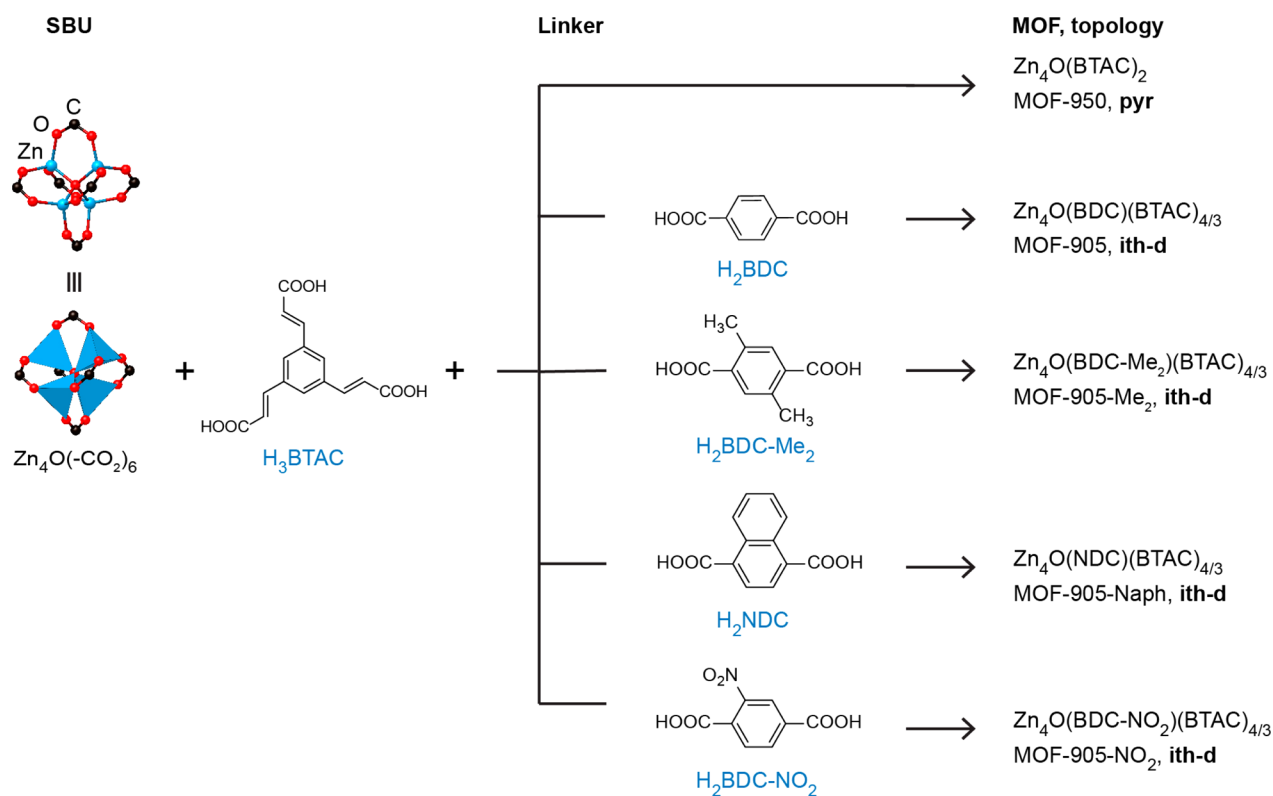
Growing interest is focused on expanding the use of methane for fueling automobiles. However, one main challenge for this expansion lies in the low energy density of methane gas under ambient conditions (0.04 MJ L⁻¹, compared to 32.4 MJ L⁻¹ for gasoline).³ Three strategies are being developed to overcome this challenge. First, the use of liquefied natural gas. Here, methane is stored under cryogenic conditions, which leads to an impressive compression to 0.16 vol % compared to gaseous methane, resulting in a high volumetric energy density of 20–23 MJ L⁻¹. However, the main drawback of this strategy is the high-cost of running a cryogenic system necessary to cool down the whole storage tank to -162 °C. To date, this technique is mainly for long distance natural gas transportation.⁴ Second, the use of compressed natural gas (CNG), where methane is stored under high pressure (200 to 250 bar) in fuel tanks attached to vehicles. Under this pressure, the volume of methane is compressed to 1 vol %, thus increasing its energy density to approximately 10 MJ L⁻¹. Vehicles using this

technology have been designed, and manufactured mainly in Europe, South America, and Asia. However, safety concerns have been raised about carrying a highly pressurized methane tank in an automobile, in case of ignition.⁵ Third, the use of adsorbed natural gas (ANG), in which methane is stored in a porous sorbent material under less extreme pressure regimes compared to CNG (below 100 bar). The superior adsorption of methane in such porous materials is expected to compensate for the loss in capacity due to operating at lower pressures. Porous carbon and newly developed MOFs are promising candidates as sorbent materials.⁶ ANG is also combined with CNG to give high pressure ANG, where a high pressure CNG tank is filled by sorbent materials. This technique aims to increase the capacity of natural gas storage and reduce the overall space occupied by the fuel tank. The presence of sorbent materials in high pressure tanks has the added benefit of making CNG a safer strategy as the desorption of methane gas from the sorbent materials takes up a significant amount of heat, cooling down the whole tank, slowing down the methane release and preventing the tank from spontaneously igniting. Vehicle models using this high pressure ANG technique have already been realized by BASF.⁷

The fast pace of development of ANG and high-pressure ANG techniques heightened the expectations for sorbent materials. In 2012, U.S. Department of Energy (DOE) updated

Received: May 22, 2016

Published: July 21, 2016

Scheme 1. $\text{Zn}_4\text{O}(-\text{CO}_2)_6$ Secondary Building Units (SBUs) Are Connected with Organic Linkers to Form MOF-950, MOF-905 and Functionalized MOF-905

the target for methane storage materials for ANG applications to a gravimetric capacity of 50 wt % and a volumetric capacity of 250 g L^{-1} .⁸ The most important parameter is the volumetric capacity, considering the limited size of an automobile fuel tank. Accordingly, new porous adsorbents are required to meet these challenging storage targets. MOFs are known to be useful in the storage of gases, including methane. Among the many MOFs studied for methane storage are HKUST-1, Ni-MOF-74, PCN-14, NOTT-101, NOTT-109, UTSA-20, UTSA-76a, Al-soc-MOF-1, and [Co(BDP), BDP = 1,4-benzenedipyrzolate], at 35 to 80 bar⁹ and MOF-5, MOF-177, MOF-205, MOF-210 at 250 bar (extrapolated data)^{10,11} have been outstanding sorbent materials, having some of the highest reported total volumetric storage capacities. Since the automobile industry requires that 5 bar of engine inlet pressure, working capacity is the key parameter to evaluate the performance of methane storage materials.^{9a} At present, the highest working capacities reported for a MOF are $155 \text{ cm}^3 \text{ cm}^{-3}$ (111 g L^{-1}), $153 \text{ cm}^3 \text{ cm}^{-3}$ (109 g L^{-1}), and $151 \text{ cm}^3 \text{ cm}^{-3}$ (108 g L^{-1}) at 35 bar for Co(BDP),^{9d} HKUST-1,^{9a} and USTA-76a,¹² respectively, and $200 \text{ cm}^3 \text{ cm}^{-3}$ (143 g L^{-1}) at 80 bar shared by HKUST-1^{9a} and Al-soc-MOF-1.^{9e}

Here, we report the synthesis, crystal structure, porosity, and methane adsorption properties for five zinc based MOFs made using organic linkers containing acrylate links [termed MOF-950: $\text{Zn}_4\text{O}(\text{BTAC})_2$, H_3BTAC = benzene-1,3,5-tri- β -acrylic acid, MOF-905: $\text{Zn}_4\text{O}(\text{BDC})(\text{BTAC})_{4/3}$, H_2BDC = 1,4-benzenedicarboxylic acid, and functionalized MOF-905: MOF-905-Me₂, MOF-905-Naph, and MOF-905-NO₂] (Scheme 1). One member of this series (MOF-905) has working capacity (desorption at 5 bar) of $203 \text{ cm}^3 \text{ cm}^{-3}$ (145 g L^{-1}) at 80 bar and 298 K, a value rivaling that of HKUST-1

($200 \text{ cm}^3 \text{ cm}^{-3}$ or 143 g L^{-1}), the benchmark compound for methane storage in MOFs.

EXPERIMENTAL SECTION

Chemicals. Pyridine ($\geq 99\%$), piperidine (99%), malonic acid (99%), acetic acid ($\geq 99\%$), sulfuric acid (95.0–98.0%), ethanol (anhydrous, $\geq 99.5\%$), zinc nitrate hexahydrate [$\text{Zn}(\text{NO}_3)_2 \cdot 6\text{H}_2\text{O}$], H_2BDC (98%), and Sigmacote siliconizing reagent were purchased from Sigma-Aldrich. 1,3,5-Triformylbenzene (98%) was obtained from Acros Organics. Anhydrous *N,N*-dimethylformamide (DMF) was obtained from EMD Millipore Chemicals. Chloroform (HPLC grade with 50 ppm pentane as a preservative) was obtained from Fisher Scientific. 2-Nitro-1,4-benzenedicarboxylic acid ($\text{H}_2\text{BDC-NO}_2$) and 2,5-dimethyl-1,4-benzenedicarboxylic acid ($\text{H}_2\text{BDC-Me}_2$) were purchased from TCI America. 1,4-Naphthalenedicarboxylic acid (H_2NDC) was obtained from Alfa Aesar. H_3BTAC was prepared according to a slightly modified published procedure.¹³ All starting materials and solvents, unless otherwise specified, were used without further purification.

Analytical Techniques. Single-crystal X-ray diffraction (SXRD) data were collected on a Bruker D8-Venture diffractometer equipped with Mo- ($\lambda = 0.71073 \text{ \AA}$) and Cu-target ($\lambda = 1.54184 \text{ \AA}$) microfocus X-ray tubes and a PHOTON 100 CMOS detector. Powder X-ray diffraction patterns (PXRD) were recorded using either a Bruker D8 Advance diffractometer (Göbel-mirror monochromated Cu $K\alpha$ radiation $\lambda = 1.54056 \text{ \AA}$) or a Rigaku Miniflex 600 diffractometer (Bragg–Brentano geometry, Cu $K\alpha$ radiation $\lambda = 1.54056 \text{ \AA}$). Elemental microanalyses (EA) were performed in the Microanalytical Laboratory of the College of Chemistry at UC Berkeley, using a PerkinElmer 2400 Series II CHNS elemental analyzer. Attenuated total reflectance (ATR) FTIR spectra of neat samples were performed in-house on a Bruker ALPHA Platinum ATR-FTIR Spectrometer equipped with a single reflection diamond ATR module. Thermal gravimetric analysis (TGA) curves were recorded in-house on a TA Q500 thermal analysis system under N_2 and air flow. Low-pressure N_2

and CH₄ adsorption isotherms were recorded in-house on Quantachrome Quadrasorb SI and Autosorb-1 volumetric gas adsorption analyzer, respectively. High-pressure methane adsorption isotherms were measured using the static volumetric method on an HPVA-100 from the VTI Corporation (currently Particulate Systems). A liquid nitrogen bath was used for adsorption measurements at 77 K. A water circulator was used for the measurements at 273, 283, and 298 K. The framework density of MOF samples was measured using a pycnometer (Ultracyc 1200e, Quantachrome). Ultrahigh-purity grade N₂, CH₄, and He (99.999% purity) gases were used throughout the gas adsorption and density measurements.

Synthesis and Characterization of MOFs. General Procedure for Sample Preparation. To reduce nucleation in the growth of MOF single crystals, the inner surface of glass containers were rinsed with Sigmacote siliconizing reagent, washed three times with acetone, and dried in oven before use. Solvent exchange of the MOFs is performed by immersing the sample in the given solvent for 3 days, during which the solvent was decanted and freshly replenished three times per day.

Zn₄O(BTAC)₂, MOF-950. A solvent mixture of H₃BTAC (0.033 g, 0.11 mmol) and Zn(NO₃)₂·6H₂O (0.25 g, 0.84 mmol) in 20 mL DMF was placed in a 20 mL screw-capped scintillation vial, which was heated at 85 °C for 3 d. Light yellow crystals were collected and quickly washed three times with 5 mL of fresh DMF. As-synthesized MOF-950 was rinsed 3 times per day with 4 mL of DMF for 3 d and immersed in 4 mL of chloroform for 3 d, during which time the solvent was replaced 3 times per day. The solid was then evacuated under dynamic vacuum, first at room temperature for 12 h and then 80 °C for 4 h to yield the activated sample (Yield: 0.029 g; 62% based on H₃BTAC). ¹H digested solution NMR of the activated sample (400 MHz, DMSO-*d*₆, ppm): 8.05 (s, 3H, 1 × BTAC), 7.60 (d, *J* = 16.1 Hz, 3H, 1 × BTAC), 6.77 (d, *J* = 16.1 Hz, 3H, 1 × BTAC). EA of activated sample: Calcd for Zn₄C₃₀H₁₈O₁₃ = Zn₄O(C₁₅H₉O₆)₂: C, 42.49; H, 2.14%. Found: C, 41.47; H, 2.09%. ATR-FTIR (4000–400 cm⁻¹): 1647 (m), 1588 (m), 1560 (sh), 1542 (sh), 1527 (m), 1444 (m), 1399 (s), 1299 (w), 1236 (w), 1166 (w), 972 (m), 895 (w), 858 (m), 753 (w), 726 (w), 670 (w), 593 (m), 524 (m), 413 (m).

Zn₄O(BDC)(BTAC)_{4/3}, MOF-905. A solvent mixture of H₃BTAC (0.045 g, 0.16 mmol), H₂BDC (0.048 g, 0.29 mmol) and Zn(NO₃)₂·6H₂O (0.26 g, 0.87 mmol) in 18 mL DMF and 1.8 mL ethanol was placed in a 20 mL screw-capped scintillation vial, which was heated at 85 °C for 1 d. Collected light yellow crystals were washed and dried in the same way as MOF-950 to yield the activated sample (Yield: 0.048 g; 49% based on H₃BTAC). ¹H digested solution NMR of activated sample (400 MHz, DMSO-*d*₆, ppm): 8.05 (s, 4H, 1.33 × BTAC), 8.03 (s, 4H, 1 × BDC), 7.60 (d, *J* = 16.1 Hz, 4H, 1.33 × BTAC), 6.77 (d, *J* = 16.1 Hz, 4H, 1.33 × BTAC). EA of activated sample: Calcd for Zn₄C₂₈H₁₆O₁₃ = Zn₄O(C₈H₄O₄)(C₁₅H₉O₆)_{4/3}: C, 40.89; H, 1.96%. Found: C, 39.87; H, 1.82%. ATR-FTIR (4000–400 cm⁻¹): 1644 (m), 1595 (m), 1535 (m), 1397 (s), 1301 (w), 1275 (w), 1236 (w), 1160 (w), 1020 (w), 983 (m), 861 (m), 825 (w), 746 (m), 666 (w), 604 (m), 576 (m), 517 (m).

Zn₄O(BDC-Me₂)(BTAC)_{4/3}, MOF-905-Me₂. A solvent mixture of H₃BTAC (0.045 g, 0.16 mmol), H₂BDC-Me₂ (0.067 g, 0.34 mmol) and Zn(NO₃)₂·6H₂O (0.26 g, 0.87 mmol) in 18 mL DMF and 1.8 mL ethanol was placed in a 20 mL screw-capped scintillation vial, which was heated at 85 °C for 1 d. Obtained light yellow crystals were washed and dried in the same way as MOF-905 to yield the activated sample (Yield: 0.044 g; 43% based on H₃BTAC). ¹H digested solution NMR of activated sample (400 MHz, DMSO-*d*₆, ppm): 8.07 (s, 4H, 1.33 × BTAC), 7.67 (s, 2H, 1 × BDC-Me₂), 7.59 (d, *J* = 16.0 Hz, 4H, 1.33 × BTAC), 6.76 (d, *J* = 16.0 Hz, 4H, 1.33 × BTAC), 2.46 (s, 6H, 1 × BDC-Me₂). EA of activated sample: Calcd for Zn₄C₃₀H₂₀O₁₃ = Zn₄O(C₁₀H₈O₄)(C₁₅H₉O₆)_{4/3}: C, 42.39; H, 2.37%. Found: C, 42.09; H, 2.02%. ATR-FTIR (4000–400 cm⁻¹): 1645 (m), 1594 (m), 1534 (m), 1400 (s), 1360 (s), 1301 (w), 1236 (w), 1194 (w), 1159 (w), 982 (m), 861 (m), 796 (w), 748 (w), 666 (w), 604 (m), 570 (w), 517 (m), 427 (w).

Zn₄O(NDC)(BTAC)_{4/3}, MOF-905-Naph. A solvent mixture of H₃BTAC (0.045 g, 0.16 mmol), H₂NDC (0.074 g, 0.34 mmol) and Zn(NO₃)₂·6H₂O (0.26 g, 0.87 mmol) in 18 mL DMF and 1.8 mL

ethanol was placed in a 20 mL screw-capped scintillation vial, which was heated at 85 °C for 1 d. Obtained light yellow crystals were washed and dried in the same way as MOF-905 to yield the activated sample (Yield: 0.047 g; 45% based on H₃BTAC). ¹H digested solution NMR of activated sample (400 MHz, DMSO-*d*₆, ppm): 8.75 (dd, *J* = 6.7 Hz, 3.4 Hz, 2H, 1 × NDC), 8.09 (s, 2H, 1 × NDC), 8.07 (s, 4H, 1.33 × BTAC), 7.69 (dd, *J* = 6.7 Hz, 3.4 Hz, 2H, 1 × NDC), 7.60 (d, *J* = 16.0 Hz, 4H, 1.33 × BTAC), 6.76 (d, *J* = 16.0 Hz, 4H, 1.33 × BTAC). EA of activated sample: Calcd for Zn₄C₃₂H₁₈O₁₃ = Zn₄O(C₁₂H₆O₄)(C₁₅H₉O₆)_{4/3}: C, 44.05; H, 2.08%. Found: C, 43.70; H, 1.98%. ATR-FTIR (4000–400 cm⁻¹): 1644 (m), 1593 (m), 1532 (m), 1400 (s), 1371 (s), 1264 (w), 1237 (w), 1165 (w), 982 (m), 860 (m), 827 (w), 789 (m), 740 (w), 666 (w), 604 (m), 587 (m), 522 (m), 472 (m).

Zn₄O(BDC-NO₂)(BTAC)_{4/3}, MOF-905-NO₂. A solvent mixture of H₃BTAC (0.045 g, 0.16 mmol), H₂BDC-NO₂ (0.062 g, 0.29 mmol) and Zn(NO₃)₂·6H₂O (0.26 g, 0.87 mmol) in 18 mL DMF and 1.8 mL ethanol was placed in a 20 mL screw-capped scintillation vial, which was heated at 85 °C for 36 h. Obtained light yellow crystals were washed and dried in the same way as MOF-905 to yield the activated sample (Yield: 0.043 g; 41% based on H₃BTAC). ¹H digested solution NMR of activated sample (400 MHz, DMSO-*d*₆, ppm): 8.24 (d, *J* = 1.4 Hz, 1H, 1 × BDC-NO₂), 8.20 (dd, *J* = 7.9 Hz, 1.4 Hz, 1H, 1 × BDC-NO₂), 8.03 (s, 4H, 1.33 × BTAC), 7.85 (d, *J* = 7.9 Hz, 1H, 1 × BDC-NO₂), 7.59 (d, *J* = 16.0 Hz, 4H, 1.33 × BTAC), 6.76 (d, *J* = 16.0 Hz, 4H, 1.33 × BTAC). EA of activated sample: Calcd for Zn₄C₂₈H₁₅NO₁₅ = Zn₄O(C₈H₃O₆N)(C₁₅H₉O₆)_{4/3}: C, 38.76; H, 1.74; N, 1.62%. Found: C, 38.98; H, 1.46; N, 1.65%. ATR-FTIR (4000–400 cm⁻¹): 1643 (m), 1615 (m), 1591 (m), 1532 (m), 1398 (s), 1302 (w), 1276 (w), 1237 (w), 1167 (w), 1133 (w), 1067 (w), 983 (m), 860 (m), 840 (w), 826 (w), 778 (w), 750 (w), 738 (w), 728 (w), 666 (w), 604 (m), 589 (m), 525 (m), 509 (m).

RESULTS AND DISCUSSION

Although several classes of adsorbent materials have been used for methane storage, it remains a challenge to find materials of high performance, especially with high volumetric working capacity.^{9a} Activated carbons have the ability to store methane at 80 bar and 298 K, however, the highest reported volumetric methane working capacities for activated carbons are in the range of 100–170 cm³ cm⁻³, well below the energy density of CNG (263 cm³ cm⁻³ at 250 bar and 298 K).^{9a}

High volumetric uptake capacity can be achieved by MOFs replete with open metal sites, as in MOF-74,¹⁴ HKUST-1,¹⁵ and PCN-14.¹⁶ These MOFs typically have high isosteric enthalpies of adsorption (*Q*_{st}) at zero coverage (17 to 21 kJ mol⁻¹) which is indicative of the significantly stronger methane-adsorbent interactions compared to those in MOFs without open metal sites (typically 10 to 15 kJ mol⁻¹).^{9a} However, as a consequence of the strong interaction with the framework, 25–40% of methane is unusable since it cannot be desorbed at 5 bar and 298 K. Furthermore, each open metal site commonly shows strong interaction with only a single methane molecule, limiting the increase in storage capacity without increasing the density of open metal sites. Thus, to achieve a high volumetric working capacity of methane under moderate storage conditions (typically between 5 and 80 bar), materials with moderate adsorption enthalpies throughout the pressure range are required.

It is generally known that inorganic secondary building units (SBUs) are the primary adsorption sites of guest molecules rather than organic linkers, even if these SBUs have no open metal sites.¹⁷ In the case of the Zn₄O(-CO₂)₆ unit, there are two type of strong binding sites on the SBU that can confine up to 8 guest molecules (i.e., α and β sites can capture 4 methane molecules respectively). However, considering the occupancy

of Ar and/or N₂ at the α and β sites of MOF-5, it is unlikely that these sites are fully occupied by methane due to the steric repulsion of adsorbed methane molecules. In contrast, highly porous Zn-based MOFs such as MOF-177 (11 × 17 Å),¹⁸ MOF-205 (DUT-6, 25 × 30 Å),^{19a,b} and MOF-210 (27 × 48 Å and 20 × 20 Å)^{19b} demonstrate high gravimetric methane uptake capacities. However, in this case, these MOFs do not exhibit saturated excess methane uptake because the average pore diameter is too large to confine methane molecules in the pore. In other words, it is important to create enough space for methane adsorption around the Zn₄O(-CO₂)₆ unit with minimal dead space, leading to the high volumetric storage capacity.²⁰

With the above considerations in mind, we decided to replace the peripheral phenylene ring of the benzene-1,3,5-tribenzoate (BTB) linker (used in MOF-177 and MOF-205) with a double-bond/triple-bond spacer. We reasoned that shrinking the individual pore sizes of these large pore MOFs, by using shorter organic linkers, will minimize the dead space without sacrificing space for adsorbed methane molecules. Given the poor thermal stability presented by carboxylates directly linking to triple-bonds,²¹ we chose to focus on the double-bond spacer version of organic linker (i.e., BTAC).

This new tricarboxylate organic linker, BTAC (Scheme 1), was synthesized by a single-step condensation of 1,3,5-triformylbenzene and malonic acid followed by in situ decarboxylation. All three double bonds generated adopt the *trans*- configuration, greatly increasing the symmetry of the H₃BTAC molecule. Reaction of the acid form of this linker with Zn(NO₃)₂·6H₂O in DMF at 85 °C for 3 d gave block crystals of MOF-950. SXRD analysis revealed that MOF-950 crystallizes in the cubic *P*2₁3 space group with the lattice constant of 21.2832(4) Å. In this structure, octahedral Zn₄O(-CO₂)₆ units are linked by tritopic BTAC linkers into a three-dimensional framework with a *pyr* topology (Figure 1), isoreticular to MOF-150 [Zn₄O(TCA)₂; TCA = 4,4',4''-tricarboxytriphenylamine]²² and MOF-155, [Zn₄O(BTB-X)₂; X = F, mNH₂].²³ However, unlike MOF-150 and MOF-155, where both consist of 2-fold interpenetrating frameworks, MOF-950 is noninterpenetrated, which leads to a bicontinuous channel with an internal pore diameter of 8.5 Å, larger than that of MOF-150 (4.5 Å) and similar to that of MOF-155 (8.5 Å) despite the shorter linker.

The use of the acid forms of ditopic (BDC) and tritopic linkers (BTAC) together with Zn(NO₃)₂·6H₂O in DMF/ethanol mixture leads to light yellow crystals of MOF-905 with truncated octahedral shape. Despite extensive trials to determine the structure from SXRD experiments, this MOF always grows in polycrystalline form, and displays weak diffraction peaks and readily degrades when exposed to ambient air. Its structure was determined by comparison of the experimental PXRD pattern with the one calculated from a structural model based on the *ith-d* net (Figure 2), with refined unit cell parameter *a* = 24.624 Å in the space group *Pm* $\bar{3}$. Like other Zn based MOFs with *ith-d* net,¹⁹ in this structure, each Zn₄O(-CO₂)₆ unit is linked to six carboxylates, four equatorial from BTAC and two axial from BDC. This results in two type of micropores present in the framework: a dodecahedral pore of 18 Å in diameter, built from four BDC and eight BTAC linkers interconnecting 12 zinc-based SBUs, and a tetrahedral pore of 6 Å in diameter, built from four zinc-based SBUs connected by two BDC and four BTAC linkers (Figure 2). Although the BTAC linker can be flexible, the ratio of the length (i.e.,

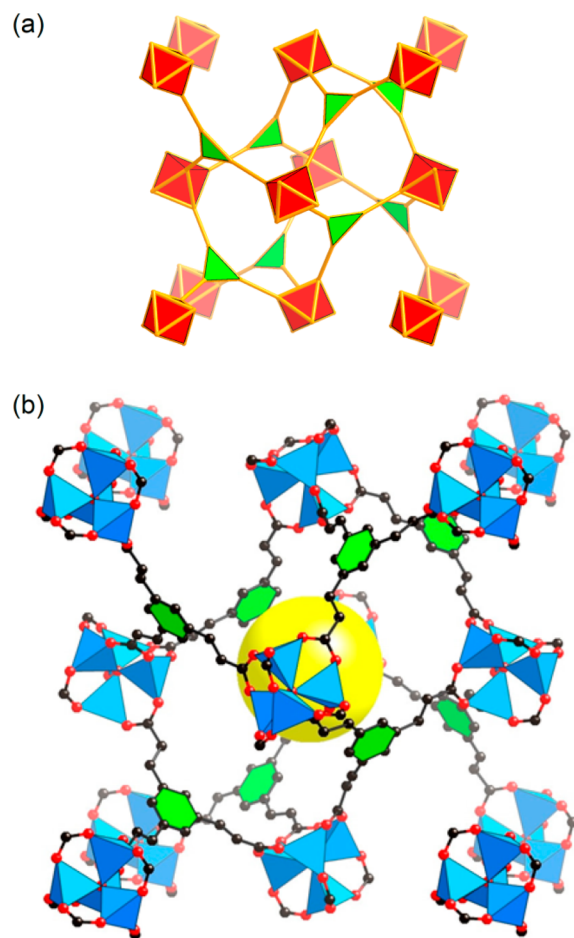


Figure 1. Combination of octahedral units with tritopic units produces the *pyr* network (a) exhibited by MOF-950 (b). Atom color scheme: C, black; O, red; Zn, blue polyhedra. H atoms are omitted for clarity. Yellow balls indicate the space in the framework.

distance between two neighboring carboxylate carbons within a single linker) between ditopic and tritopic linkers for MOF-905 (0.63) is similar to MOF-205 (0.64).^{9b} As expected, the size of the larger cages in MOF-905 (18.0 Å) is smaller than that of MOF-205 (25.0 Å), while the size of the smaller cages for MOF-905 (6.0 Å) is even larger than that of MOF-205 (5.0 Å) (Table 1). This indicates that the shorter BTAC linker is able to effectively reduce the dead space, making it a good candidate to achieve high volumetric storage capacity at 80 bar.

We were interested in the role of functional groups in these MOFs and their methane storage capacities, which motivated us to construct a series of highly porous MOFs that have well-separated functionalized linkers. Three functionalized MOF-905 (MOF-905-Me₂, MOF-905-Naph, and MOF-905-NO₂) were obtained with the same synthetic method, using the acid forms of ditopic BDC-Me₂, NDC, and BDC-NO₂ linkers instead of BDC (Scheme 1). Similar to MOF-905, structural determination of these functionalized MOFs by single crystal diffraction techniques was not successful. Instead, their structure and phase purity were confirmed by comparing their experimental PXRD patterns with simulated ones from structural models (SI, Sections S2 and S3). It should be noted that the diameter of larger cages for a series of functionalized MOF-905 ranges from 15.3 to 17.6 Å (for MOF-905-Naph and -Me₂, respectively), while the diameter of smaller cages is still greater than that of expanded version, MOF-205 (Table 1).

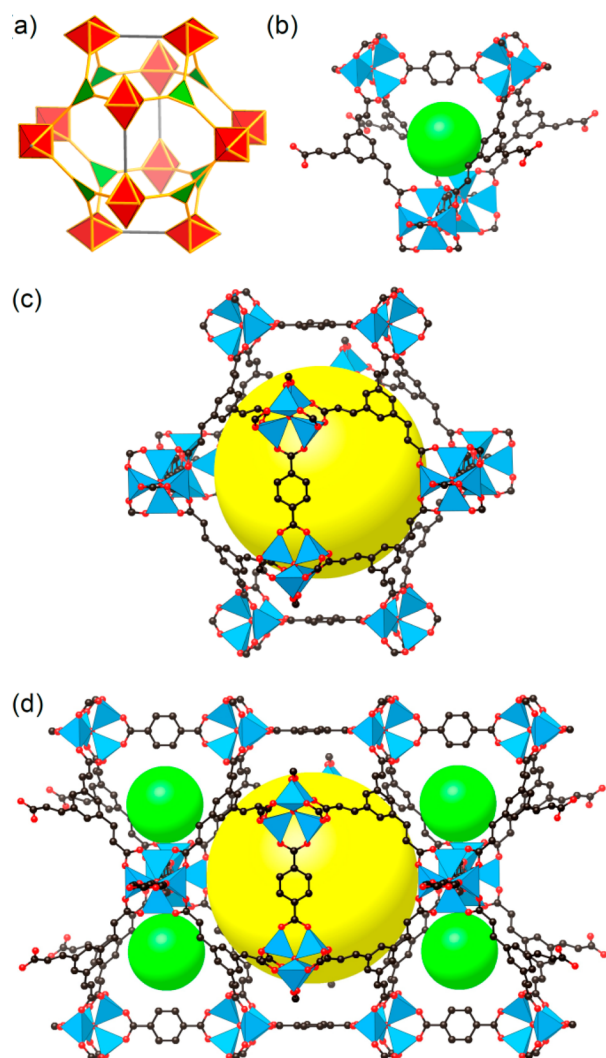


Figure 2. Combination of octahedral units with ditopic and tritopic units produces the *ith-d* network (a) with tetrahedral (b) and octahedral cages (c) exhibited in MOF-905 (d). Atom color scheme: C, black; O, red; Zn, blue polyhedra. H atoms are omitted for clarity. Yellow and green balls indicate the space in the framework.

Porosity of MOFs. Prior to the methane adsorption tests, N_2 adsorption isotherms for all five MOFs were recorded at 77 K to confirm the presence of permanent porosity and to calculate their pore volume (Table 1). The guest-free (activated) materials were obtained by solvent exchange with

chloroform followed by direct evacuation of pores under dynamic vacuum (4×10^{-5} bar). Successful removal of guest molecules from the pore was also confirmed by thermogravimetric analysis (SI, Section S4). All examined MOFs displayed significant N_2 uptake in the low pressure region ($P/P_0 < 0.05$) and were saturated around $P/P_0 = 0.2$ (SI, Figures S12 to S16). The profiles of the isotherms are all classified as Type I and the adsorption of N_2 was fully reversible, which is characteristic of permanent microporosity. Compared to MOF-905, the functionalized MOF-905 materials show slightly lower N_2 uptake because the presence of extra functional groups reduces the pore volume. All of these materials exhibit high BET surface areas ($>3000 \text{ m}^2 \text{ g}^{-1}$) and large pore volumes (ca. $1.3 \text{ cm}^3 \text{ g}^{-1}$), which are in good agreement with those calculated from their structural models. The BET (Langmuir) surface area, pore volume, crystal density, and pore diameter are summarized along with other benchmark MOFs with the $Zn_4O(-CO_2)_6$ SBU in Table 1.

Low-Pressure Methane Isotherms and Adsorption Enthalpies. Low-pressure methane uptake isotherms for MOF-950, MOF-905, and functionalized MOF-905 were measured up to 1.1 bar at 273, 283, and 298 K (SI, Figures S17–S21). Methane uptake in these MOFs increases linearly with pressure, with no saturation in uptake observed in the pressure region studied. Methane uptake for these new MOFs at 298 K and 1.1 bar ranges from $8.1 \text{ cm}^3 \text{ g}^{-1}$ (MOF-905- NO_2) to $11.0 \text{ cm}^3 \text{ g}^{-1}$ (MOF-905- Me_2), and these are comparable to the methane uptake in MOF-177 ($9.1 \text{ cm}^3 \text{ g}^{-1}$) under the same conditions (Table 1). Such moderate methane uptake capacity below 1.1 bar should be advantageous in achieving a larger working capacity for practical natural gas storage processes. It is known that low-pressure methane adsorption capacity correlates to the adsorption enthalpy rather than porosity of sorbent materials. Accordingly, the isosteric enthalpy of adsorption (Q_{st}) for methane was calculated based on methane isotherms collected at 273, 283, and 298 K.

Figure S22 demonstrates the coverage dependencies of Q_{st} calculated from fitting these data. MOF-950 shows slightly higher near-zero coverage Q_{st} value than MOF-905 (11.9 and 11.7 kJ mol^{-1} , respectively); however, the profile of these Q_{st} curves is nearly flat in the low coverage region. We note that these Q_{st} values are comparable to those in MOF-5 (12.3 kJ mol^{-1}), MOF-177 (9.9 kJ mol^{-1}), and MOF-205 (10.6 kJ mol^{-1}), MOFs with $Zn_4O(-CO_2)_6$ SBUs; but less than those of Ni-MOF-74 (21.4 kJ mol^{-1}), PCN-14 (18.7 kJ mol^{-1}), and HKUST-1 (17.0 kJ mol^{-1}), MOFs with open metal sites.^{9a} Considering that the Q_{st} values of MOFs with $Zn_4O(-CO_2)_6$

Table 1. Summary of the Low-Pressure Sorption, Physical and Pore-Structure Properties of the Studied Zinc MOFs

material	surface area, $\text{m}^2 \text{ g}^{-1}$		$V_{p\prime}$ ^a $\text{cm}^3 \text{ g}^{-1}$	d_{crystal} ^b g cm^{-3}	d_{pycnor} ^c g cm^{-3}	D , ^d Å	CH_4 uptake, ^e $\text{cm}^3 \text{ g}^{-1}$	Q_{st} , kJ mol^{-1}
	BET	Langmuir						
MOF-905	3490	3770	1.34	0.549	0.537	6.0, 18.0	7.7	11.7
MOF-905- Me_2	3640	3920	1.39	0.568	0.515	5.5, 17.6	11.0	10.3
MOF-905-Naph	3310	3540	1.25	0.585	0.553	6.8, 15.3	10.2	11.3
MOF-905- NO_2	3380	3600	1.29	0.580	0.551	5.1, 17.3	8.1	10.7
MOF-950	3440	3650	1.30	0.517	0.540	8.5	8.6	11.9
MOF-205	4080	5700	1.96	0.380	0.402	5.0, 25.0	8.0	10.6
MOF-177	4700	5060	1.83	0.427	0.411	10.8	9.1	9.9
MOF-5	3480	3860	1.39	0.605	0.533	12.8	7.3	10.0

^aCalculated from uptake at $P/P_0 = 0.9$. ^bFrom crystal structure and model structure data. ^cFrom pycnometer density data, averaged from 10 measurements on multiple batches of samples. ^dPore diameter calculated with Platon.²⁴ ^eData at 1.1 bar and 298 K.

SBUs are not substantially influenced by the surface coverage of methane, it is presumed that primary methane adsorption sites should be located near the SBU.

Compared to MOF-905, three functionalized MOF-905 materials show lower Q_{st} values of 10.3 (–Me₂), 11.3 (–Naph), and 10.7 (–NO₂) kJ mol^{–1}, although it is proposed that methyl functionalities can have a positive impact on the methane adsorption.²⁵ Assuming that the primary methane adsorption sites are nearby the Zn₄O(–CO₂)₆ SBUs at ambient pressure, it is likely that the introduced methyl functionalities can block access of methane to the primary adsorption site rather than enhance the adsorbate–adsorbent interactions based on the functionalization of the benzene with electron donating groups. This is in contrast to the trend that Me and Cl functionalized Zn-based MOFs show higher Q_{st} .²⁶ However, these MOFs have relatively small pore diameter (ca. 7 Å) such that the increased Q_{st} values can be attributed to the pore size effect.

High-Pressure Methane Storage. High-pressure excess methane isotherms (up to 80 bar) for MOF-950, MOF-905, and functionalized MOF-905 were recorded at 298 K on a volumetric adsorption analyzer to evaluate the storage performance of methane (Figure 3a). Methane uptake in these MOFs

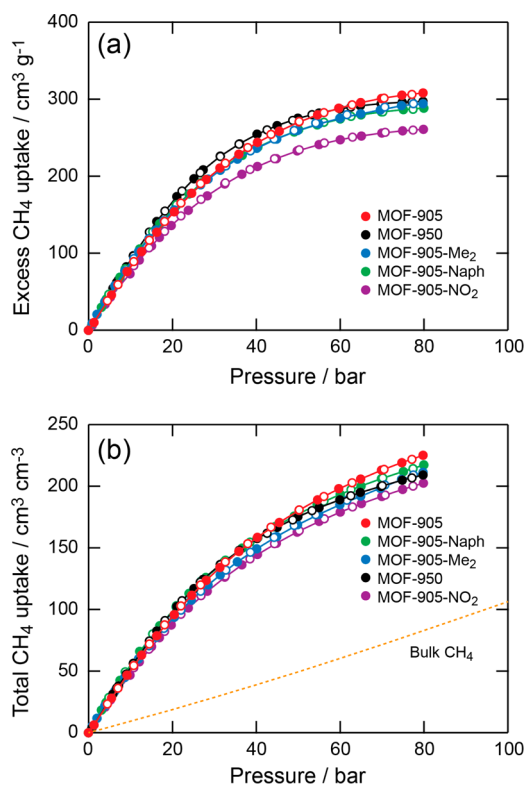


Figure 3. Excess (a) and total (b) CH₄ isotherms for MOFs measured at 298 K.

gradually increases with increasing pressure. Methane uptake below 20 bar is similar, while MOF-950 with the smallest pore diameter among Zn-based MOF showed the highest methane uptake in the medium pressure range (20–50 bar). By increasing pressure further, excess uptake in each case is approaching saturation. The excess uptake at 80 bar and 298 K is nearly proportional to the surface area (pore volume) of MOFs. MOF-905 showed the highest methane uptake of 310 cm³ g^{–1} and this is followed by MOF-950 (297 cm³ g^{–1}), MOF-905-Me (294 cm³ g^{–1}), MOF-905-Naph (289 cm³ g^{–1}), and

MOF-905-NO₂ (261 cm³ g^{–1}). Volumetric excess methane uptake can be calculated by multiplying the bulk density of materials. However, experimental bulk density cannot be the same as the theoretical one calculated from the crystal structure when the MOF sample is poorly activated or contains defect sites in its structure. Therefore, prior to unit conversion, we sought to estimate the bulk density of these MOFs using skeletal density ($d_{skl} = 1/V_{skl}$) and pore volume (V_p), because these are experimentally determined using He pycnometry and N₂ adsorption, respectively:

$$\text{experimental bulk density} = 1/(1/d_{skl} + V_p) \quad (1)$$

As demonstrated in Table 1, the experimental bulk density for these MOFs was 5–10% lower compared to the theoretical crystal density, which is indicative of the presence of defects in the MOF crystals. The maximum excess methane uptake for MOF-905 in volumetric units is 167 cm³ cm^{–3} at 80 bar and 298 K, which outperforms MOF-950 (153 cm³ cm^{–3}) and functionalized MOF-905 (160, 151, and 144 cm³ cm^{–3} for –Naph, –Me₂, and –NO₂, respectively).

To explore the potential as sorbent materials in their practical application, the total methane uptake in volumetric units is commonly used. Accordingly, the total uptake was calculated from the excess methane uptake using the following equation:

$$N_{\text{total}} = N_{\text{excess}} + \rho_{\text{CH}_4} \times V_p \quad (2)$$

As shown in Figure 3b, calculated total methane uptake monotonously increases with pressure, with no saturation behavior observed. The total volumetric methane uptake for MOF-950, MOF-905, and functionalized MOF-905 at 80 bar and 298 K are ranging from 203 (MOF-905-NO₂) to 228 cm³ cm^{–3} (MOF-905). Remarkably, methane uptake in MOF-905 at 80 bar is 2.7 times larger than bulk methane density at the same temperature and pressure. This value is also 10% greater than MOF-177 (205 cm³ cm^{–3}) and larger-pore MOF-205 (205 cm³ cm^{–3}), and is approaching the best performing MOFs, such as HKUST-1 (272 cm³ cm^{–3} at 80 bar)¹⁰ and UTSA-76a (257 cm³ cm^{–3} at 65 bar).¹²

Effect of Pore Size and Functionality. To validate our hypothesis that methane storage capacity is enhanced by reducing the diameter of the large cages in low density MOFs, such as MOF-177 and MOF-205, the total volumetric methane uptakes for Zn-MOFs at 298 K were also compared. In the case of single linker MOFs, as shown in Table 2, the total volumetric uptake in MOF-950 outperforms MOF-177 in the entire range of 35 to 80 bar.²⁸ Similar trend was observed for the mixed linker system: in the entire range of 35 to 80 bar, the smaller pore MOF-905 showed 11 to 21% enhancement on total volumetric methane uptake over larger-pore MOF-205. These results combined clearly indicate a significant benefit of proper pore size on total methane storage capacity at these pressures.

The addition of organic functional groups may have an extra influence on total volumetric methane uptake at high pressure. At 35 bar, MOF-905-Naph exhibits the highest total volumetric methane uptake among four MOF-905 materials, followed by MOF-905, MOF-905-Me₂, and MOF-905-NO₂. However, the benefits from introducing organic functionality disappear with increasing pressure from 35 to 80 bar (Table 2). At 35 bar, the total volumetric methane uptake of MOF-905-Naph (146 cm³ cm^{–3}) is comparable to that of MOF-905 (145 cm³ cm^{–3}),

Table 2. Summary of MOF Net, Pore Size, And Total Methane Uptake and Working Capacity (Desorption at 5 bar) at 35 and 80 bar and 298 K²⁷

material	net	D_p^a , Å	total uptake at 35 bar, $\text{cm}^3 \text{cm}^{-3}$	total uptake at 80 bar, $\text{cm}^3 \text{cm}^{-3}$	working capacity at 35 bar, $\text{cm}^3 \text{cm}^{-3}$	working capacity at 80 bar, $\text{cm}^3 \text{cm}^{-3}$
MOF-905	ith-d	6.0, 18.0	145	228	120	203
MOF-905-Me ₂	ith-d	5.5, 17.6	138	211	111	184
MOF-905-Naph	ith-d	6.8, 15.3	146	217	117	188
MOF-905-NO ₂	ith-d	5.1, 17.3	132	203	107	177
MOF-950	pyr	8.5	145	209	109	174
MOF-5 ^b	pcu	12.8	126	198	104	176
MOF-177 ^b	qom	10.8	122	205	102	185
MOF-205 ^b	ith-d	5.0, 25.0	120	205	101	186
MOF-210 ^b	toz	20, 27 × 40	82	166	70	154
Ni-MOF-74 ^c	etb	13.6	230	267	115	152
HKUST-1 ^c	tbo	4, 10, 11	225	272	153	200
Al-soc-MOF-1 ^d	edq/ soc	14.3	127	221	106	201
PCN-14 ^e	fof/nbo	14.3	200	250	128	178
UTSA-76a ^e	fof/nbo	10.2, 9.6 × 22.3	211	257 ^f	151	197 ^f
Co(BDP) ^g	oab	2.6–8.0	161	203 ^f	155	197 ^f
MOF-519 ^h	sum	7.6	200 ^h	279 ^h	151 ^h	230 ^h
AX-21 ^c	n/a	n/a	153	222	103	172
Bulk CH ₄	n/a	n/a	33	83	29	79

^aCalculated with Platon.²⁴ ^bData from ref 10. ^cData from ref 9a. ^dData from ref 9e. ^eData from ref 12. ^fData measured at 298 K and 65 bar. ^gData from ref 9d. ^hWe note that the difficulty in controlling the composition of synthesized MOF-519 has led to poor reproducibility and likely overestimation of these reported values.

while at 80 bar, the total volumetric methane uptake of MOF-905-Naph is 5% lower than that of MOF-905.

Methane Storage Working Capacity. Considering the practical application of methane storage in automobiles, the volumetric working capacity of methane (desorption pressure is at 5 bar) was also obtained, as shown in Table 2. Due to MOF-905's moderate Q_{st} for methane, only $25 \text{ cm}^3 \text{ cm}^{-3}$ of adsorbed methane is unusable at desorption pressure of 5 bar. This value is slightly greater than those for larger pore MOF-205 and MOF-177 (19 and $20 \text{ cm}^3 \text{ cm}^{-3}$, respectively), but significantly lower compared to HKUST-1 ($72 \text{ cm}^3 \text{ cm}^{-3}$). This allows MOF-905 to extend its advantage over larger pore MOFs from total volumetric methane uptake to volumetric methane storage working capacity; at the same time to compete with MOFs with open metal sites. Indeed, the working capacity of MOF-905 at 35 bar is $120 \text{ cm}^3 \text{ cm}^{-3}$, while at 80 bar this MOF is able to deliver $203 \text{ cm}^3 \text{ cm}^{-3}$, which surpasses all other zinc-based MOFs, including the larger-pore MOF-205 ($101 \text{ cm}^3 \text{ cm}^{-3}$ at 35 bar and $186 \text{ cm}^3 \text{ cm}^{-3}$ at 80 bar) and MOF-177 ($102 \text{ cm}^3 \text{ cm}^{-3}$ at 35 bar and $185 \text{ cm}^3 \text{ cm}^{-3}$ at 80 bar). More significantly, this value is comparable to the benchmark compound HKUST-1 ($200 \text{ cm}^3 \text{ cm}^{-3}$) at 80 bar. We note that at 80 bar, a tank filled with MOF-905 would deliver 2.5 times more methane than a tank containing no sorbent material.

■ ASSOCIATED CONTENT

● Supporting Information

The Supporting Information is available free of charge on the ACS Publications website at DOI: 10.1021/jacs.6b05261.

Crystallographic data (CIF)

Structure model details, crystal structure refinement tables, PXRD patterns, thermal gravimetric curves, gas adsorption isotherms (PDF)

■ AUTHOR INFORMATION

Corresponding Author

*yaghi@berkeley.edu

Author Contributions

‡J.J. and H.F. contributed equally.

Notes

The authors declare no competing financial interest.

■ ACKNOWLEDGMENTS

The research was supported by BASF SE (Ludwigshafen, Germany). We acknowledge Prof. M. W. Deem and Mr. Y. Bao (Rice University), and Mr. C. A. Trickett from the Yaghi group for invaluable discussions.

■ REFERENCES

- (1) U.S. Energy Information Administration, Annual Energy Outlook, 2015. [http://www.eia.gov/forecasts/aeo/pdf/0383\(2015\).pdf](http://www.eia.gov/forecasts/aeo/pdf/0383(2015).pdf). (Accessed on June 26, 2016).
- (2) U.S. Energy Information Administration, Natural Gas Annual, 2014. http://www.eia.gov/naturalgas/annual/pdf/table_002.pdf. (Accessed on June 26, 2016).
- (3) Alternative Fuels Data Center, Fuel Properties Comparison, 2013. http://www.afdc.energy.gov/fuels/fuel_comparison_chart.pdf. (Accessed on June 26, 2016).
- (4) Menon, V. C.; Komarneni, S. *J. Porous Mater.* **1998**, *5*, 43–58.
- (5) (a) Talu, O. *Proc. 4th Int. Conf. on Fundamentals of Adsorption*, Kyoto, 1992; 655;. (b) Yeh, S. *Energy Policy* **2007**, *35*, S865–S875.
- (c) Whyatt, G. A. *Issues Affecting Adoption of Natural Gas in Light- and Heavy-Duty Vehicles*, 2010; PNNL-19745.
- (6) (a) Wegrzyn, J.; Gurevich, M. *Appl. Energy* **1996**, *55*, 71–83.
- (b) Judd, R. W.; Gladding, D. T. M.; Hodrien, R. C.; Bates, D. R.; Ingram, J. P.; Allen, M. *Prepr. Pap. Am. Chem. Soc. Div. Fuel Chem.* **1998**, *43*, S75–S79.
- (c) Dvorak, K.; Hodrien, R. C. Development of Adsorbed Natural Gas Technology for Large Scale Diurnal Storage Applications; Int. Gas Research Conference, Amsterdam, 2001.
- (d) Lau, L. Y.; Judd, R. W. New Approach to Natural Gas

Storage—Advances in Adsorbed Natural Gas (ANG) Technology; Int. Gas Research Conference, Paris, 2008.

(7) Furukawa, H.; Müller, U.; Yaghi, O. M. *Angew. Chem., Int. Ed.* **2015**, *54*, 3417–3430.

(8) *Methane Opportunities for Vehicular Energy*, Advanced Research Project Agency – Energy, U.S. Dept. of Energy, Funding Opportunity no. DE-FOA-0000672. <https://arpa-e-foa.energy.gov/Default.aspx?Search=DE-FOA-0000672>. (Accessed on June 26, 2016).

(9) (a) Mason, J. A.; Veenstra, M.; Long, J. R. *Chem. Sci.* **2014**, *5*, 32–51. (b) He, Y.; Zhou, W.; Qian, G.; Chen, B. *Chem. Soc. Rev.* **2014**, *43*, 5657–5678. (c) Peng, Y.; Krungleviciute, V.; Eryazici, I.; Hupp, J. T.; Farha, O. K.; Yildirim, T. *J. Am. Chem. Soc.* **2013**, *135*, 11887–11894. (d) Mason, J. A.; Oktawiec, J.; Taylor, M. K.; Hudson, M. R.; Rodriguez, J.; Bachman, J. E.; Gonzalez, M. I.; Cervellino, A.; Guagliardi, A.; Brown, C. M.; Llewellyn, P. L.; Masciocchi, N.; Long, J. R. *Nature* **2015**, *527*, 357–361. (e) Alezi, D.; Belmabkhout, Y.; Suyetin, M.; Bhatt, P. M.; Weseliński, Ł. J.; Solovyeva, V.; Adil, K.; Spanopoulos, I.; Trikalitis, P. N.; Emwas, A.-H.; Eddaoudi, M. *J. Am. Chem. Soc.* **2015**, *137*, 13308–13318.

(10) Gándara, F.; Furukawa, H.; Lee, S.; Yaghi, O. M. *J. Am. Chem. Soc.* **2014**, *136*, 5271–5274.

(11) Volumetric storage capacities for 250 bar were extrapolated with a dual site Langmuir model.

(12) Li, B.; Wen, H.-M.; Wang, H.; Tyagi, M.; Yildirim, T.; Zhou, W.; Chen, B. *J. Am. Chem. Soc.* **2014**, *136*, 6207–6210.

(13) Ried, W.; Königstein, F.-J. *Chem. Ber.* **1959**, *92*, 2532–2542.

(14) (a) Rosi, N. L.; Kim, J.; Eddaoudi, M.; Chen, B.; O’Keeffe, M.; Yaghi, O. M. *J. Am. Chem. Soc.* **2005**, *127*, 1504–1518. (b) Dietzel, P. D. C.; Panella, B.; Hirscher, M.; Blom, R.; Fjellvåg, H. *Chem. Commun.* **2006**, 959–961.

(15) Chui, S. S. Y.; Lo, S. M. F.; Charmant, J. P. H.; Orpen, A. G.; Williams, I. D. *Science* **1999**, *283*, 1148–1150.

(16) Ma, S.; Sun, D.; Simmons, J. M.; Collier, C. D.; Yuan, D.; Zhou, H.-C. *J. Am. Chem. Soc.* **2008**, *130*, 1012–1016.

(17) Rowsell, J. L. C.; Spencer, E. C.; Eckert, J.; Howard, J. A. K.; Yaghi, O. M. *Science* **2005**, *309*, 1350–1354.

(18) Chae, H. K.; Siberio-Perez, D. Y.; Kim, J.; Go, Y.-B.; Eddaoudi, M.; Matzger, A. J.; O’Keeffe, M.; Yaghi, O. M. *Nature* **2004**, *427*, 523–527.

(19) (a) Klein, N.; Senkovska, I.; Gedrich, K.; Stoeck, U.; Henschel, A.; Mueller, U.; Kaskel, S. *Angew. Chem., Int. Ed.* **2009**, *48*, 9954–9957. (b) Furukawa, H.; Ko, N.; Go, Y. B.; Aratani, N.; Choi, S. B.; Choi, E.; Yazaydin, A. O.; Snurr, R. Q.; O’Keeffe, M.; Kim, J.; Yaghi, O. M. *Science* **2010**, *329*, 424–428. (c) Liu, L.; Konstas, K.; Hill, M. R.; Telfer, S. G. *J. Am. Chem. Soc.* **2013**, *135*, 17731–17734. (d) Spanopoulos, I.; Xydias, P.; Malliakas, C. D.; Trikalitis, P. N. *Inorg. Chem.* **2013**, *52*, 855–862. (e) Sim, J.; Yim, H.; Ko, N.; Choi, S. B.; Oh, Y.; Park, H. J.; Park, S. Y.; Kim, J. *Dalton Trans.* **2014**, *43*, 18017–18024. (f) Helten, S.; Sahoo, B.; Bon, V.; Senkovska, I.; Kaskel, S.; Glorius, F. *CrystEngComm* **2015**, *17*, 307–312. (g) Liu, L.; Telfer, S. G. *J. Am. Chem. Soc.* **2015**, *137*, 3901–3909.

(20) Song, C.; Ling, Y.; Feng, Y.; Zhou, W.; Yildirim, T.; He, Y. *Chem. Commun.* **2015**, *51*, 8508–8511.

(21) Münch, A. S.; Katzsch, F.; Weber, E.; Mertens, F. O. R. L. *J. Mol. Struct.* **2013**, *1043*, 103–108.

(22) Chae, H. K.; Kim, J.; Friedrichs, O. D.; O’Keeffe, M.; Yaghi, O. M. *Angew. Chem., Int. Ed.* **2003**, *42*, 3907–3909.

(23) Zhang, Y.-B.; Furukawa, H.; Ko, N.; Nie, W.; Park, H. J.; Okajima, S.; Cordova, K. E.; Deng, H.; Kim, J.; Yaghi, O. M. *J. Am. Chem. Soc.* **2015**, *137*, 2641–2650.

(24) Spek, A. L. *Acta Crystallogr., Sect. D: Biol. Crystallogr.* **2009**, *D65*, 148–155.

(25) Wilmer, C. E.; Leaf, M.; Lee, C. Y.; Farha, O. K.; Hauser, B. G.; Hupp, J. T.; Snurr, R. Q. *Nat. Chem.* **2011**, *4*, 83–89.

(26) Wang, Y.; Tan, C.; Sun, Z.; Xue, Z.; Zhu, Q.; Shen, C.; Wen, Y.; Hu, S.; Wang, Y.; Sheng, T.; Wu, X. *Chem. - Eur. J.* **2014**, *20*, 1341–1348.

(27) Three batches of MOF-905 were prepared and measured for their methane storage properties. Results were consistent with the ones reported as shown in SI (Figure S28).

(28) The calculated density of **qom** and **pyr** nets, where hexagonal nodes are connected with the same length of linker, is exactly the same. Although the comparison of methane uptake properties for MOF-177 and MOF-950 is not ideal, this should still be a good guide to assess the pore diameter effect.